

A note on the radiance distributions of halos due to scattering by randomly orientated crystals

Gunther P. Können

Sophialaan 4, NL-3761DK Soest, The Netherlands (konnen@planet.nl)

Received 14 July 2014; revised 24 September 2014; accepted 24 September 2014;
posted 25 September 2014 (Doc. ID 216955); published 9 January 2015

The radiance distribution of light scattered by randomly oriented ice crystals differs fundamentally from the radiance distribution of light scattered by spherical raindrops or by preferentially oriented ice crystals. A formalism for light scattering by randomly oriented crystals is given and applied to four examples, among them the circular 22° halo and the antisolar halospot, the latter being the glory analogue for ice crystals. A long-standing misconception about the nature of the radiance distribution of circular halos is quantified and discussed. © 2015 Optical Society of America

OCIS codes: (010.1290) Atmospheric optics; (010.2940) Ice crystal phenomena; (290.5850) Scattering, particles; (290.5825) Scattering theory.
<http://dx.doi.org/10.1364/AO.54.00B177>

1. Introduction: Halos and Rainbows

A powerful approach to analyze special features in scattering patterns is to factorize the geometrical-optics differential cross section $d\sigma/d\Omega$ (often denoted in papers about halos or rainbows by I and then loosely called the “radiance” [1]) into a factor D that takes the scattering geometry into account and is called by various authors [2,3] the “divergence” [4], and a transmission factor $T \leq 1$ that describes the loss in intensity during the interaction with the particle [2,3,5,6]. Assuming cylindrical symmetry in the scattering geometry,

$$I \equiv \frac{d\sigma}{d\Omega} = T(b)D \equiv T(b) \frac{b}{\sin(\theta)} \left| \frac{db}{d\theta} \right|, \quad (1)$$

(see Fig. 1) in which θ is the scattering angle, b is the impact parameter (i.e., the distance of the incoming light ray from the symmetry axis), and $\theta(b)$ is called the deflection function.

T depends on the light path via the scatterer (often a sphere is considered) and is a function of the Fresnel coefficients for refraction and reflection.

Attention is usually focused on situations in Eq. (1) where $D(\theta)$ possesses a singularity: to axial focusing (glory scattering) for $\theta = 0, 180^\circ$, and to $\theta'(b) = 0$ (causing caustics; see [7–12] for examples in particle scattering). The divergence $D(\theta)$ provides a fair representation of $I(\theta)$ near such singularities as long as T depends only weakly on b in the interval of interest, which is usually the case (but see [13]).

The ordinary rainbow emerges when $\theta'(b) = 0$ and $\theta''(b) \neq 0$. Then the deflection function can be expanded as

$$\theta(b) = \theta_r + C(b - b_r)^2, \quad (2)$$

where θ_r and b_r refer to the values at the rainbow angle and where C is constant. With Eq. (1), this yields for the geometric-optics radiance distribution of the rainbow on its bright side (which we assume here to be at $\theta > \theta_r$) the well-known inverse square-root distribution:

$$I_{\text{rainbow}}(\theta) \propto (\theta - \theta_r)^{-\frac{1}{2}}. \quad (3)$$

For refraction halos, which emerge from the passage of light through an ice prism, often a formula similar to Eq. (1) is applied (see, e.g., [5]):

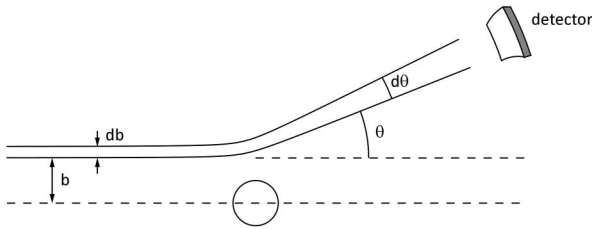


Fig. 1. After the interaction with a particle, light rays that had entered in an area $2\pi bdb$ are scattered into a solid angle $2\pi \sin(\theta)d\theta$. The divergence D is the ratio of these two terms.

$$I_{\text{halo}}(\theta) = T(i) \left| \frac{di}{d\theta} \right|, \quad (4)$$

where i is the angle of incidence at the prism and where the prism axis is implicitly assumed to have a fixed angle with the Sun. The parameter T depends on the Fresnel factors and on geometrical shielding of the light rays by the faces of the crystals. On rotating a prism about its axis, the deflection function $\theta(i)$ reaches a minimum value θ_{min} at i_{min} . Using an expansion like Eq. (2) and noting that the dependency of T on i can be in first order neglected, one finds for the halo radiance distribution near θ_{min}

$$I_{\text{halo}}(\theta) \propto (\theta - \theta_{\text{min}})^{-\frac{1}{2}}, \quad (5)$$

which is the same as the inverse square-root formula that describes the geometric-optics radiance distribution of rainbows Eq. (3).

Equations (4) and (5) apply well to parhelia and to the caustics of two-dimensional [14] refraction halos (called by Berry and Klein [15] “fake caustics” to distinguish them from the “genuine” ones like those in drops), among them the upper and lower tangent arcs to the 22° halo and the infra- and supralateral arcs to the 46° halo. However, as hinted at qualitatively by Tricker in 1970 [16] in a discussion about halo colors, stated more explicitly by Tape in 1980 [14] in his paper about halo caustics and derived quantitatively by me [17] in 1983 during an analysis of radiance distribution of the circular 22° halo, Eqs. (4) and (5) fail to describe scattering by randomly oriented crystals. The reason is that D differs fundamentally from the cases described above, which leads to radiance distributions that differ fundamentally from those encountered in light scattering by drops or by preferentially oriented crystals—a fact that has been often overlooked in studies about halos.

In this paper, I present a general formalism for light scattering by randomly oriented crystals. The purpose is conceptual for obtaining a better understanding of halos, and in this way to complement the computer approach to halos. The formalism is worked out for geometric optics. Special features of the radiance distributions of four halos arising from scattering of light by randomly oriented crystals are explicitly calculated and discussed. With the inclusion of an analysis of the parhelion radiance, emphasis is given to the difference in the radiance

distribution of circular halos if calculated with the correct formalism instead of being obtained from an often-applied misconstrued model of formation.

2. Divergence D and Halo Radiance I for Randomly Oriented Crystals

The concept of divergence for halos differs from that for rainbows since the impact parameter is no longer relevant. For the derivation of the divergence for randomly oriented crystals D_{ran} , we introduce the *deflection sphere* of a light-scattering crystal. Its construction is as follows. First, the crystal is fixed in a Cartesian frame with coordinates uvw . Around the center a unit sphere S^2 is defined. The spherical coordinates of a point s on the sphere are denoted by (ϑ, φ) . Each point s on the sphere represents a possible position of the Sun, as seen in the crystal frame.

Now we choose a light path from Sun to observer via the crystal—for instance via a simple external reflection at a crystal face or via refraction through a 60° wedge of two prism faces of a hexagonal ice crystal. For this prescribed path, we calculate for any s the scattering angle $\theta_0(s)$. Then we vary s over the sphere and draw a contour map of points with equal θ_0 . This is the deflection sphere of the crystal—or, more precisely, of the chosen light path through the crystal. Figure 2 shows the deflection sphere for external reflection.

Random orientation is assumed. Hence all surface elements $d\omega$ on the deflection sphere have the same probability to momentarily contain the Sun direction. From this, it follows that the probability that the crystal is in an orientation for scattering light

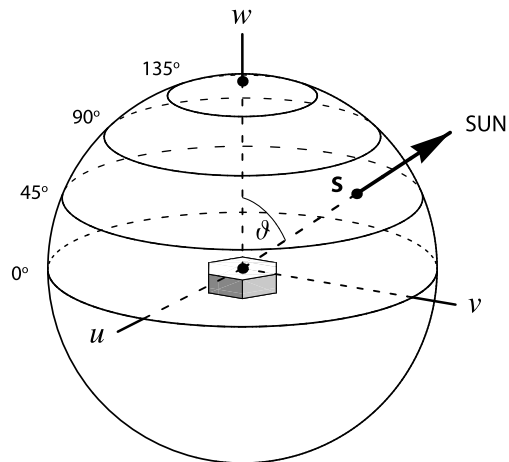


Fig. 2. Deflection sphere for external reflection at the top face of an ice crystal. The crystal is fixed in a uvw Cartesian frame. Any point s on the sphere represents a possible position of the Sun as seen from the crystal; the positive w axis is chosen here to coincide with face normal of the reflecting face. The vector gives a momentary realization of the position of the true Sun by the randomly oriented crystal; the colatitude of that realization is ϑ . To each point s on the upper hemisphere corresponds a scattering angle θ , which is the angle between the Sun and the halo point (here the negative of the reflected ray). The contours are isolines of equal scattering angle.

in a direction between angle θ and $\theta + d\theta$ is the surface area on the deflection sphere between these contours, divided by 4π . This light is scattered into a solid angle $2\pi \sin(\theta)d\theta$ whose probability is $(2\pi \sin(\theta)d\theta)/4\pi$. The divergence at θ is the ratio of these probabilities.

Denoting the area on the deflection sphere where the scattering angle is less or equal than a given value θ_0 by $A(\theta_0)$,

$$A(\theta_0) = \text{area of } \{s \in S^2 : \theta \leq \theta_0\} \quad (6)$$

gives for the divergence

$$D_{\text{ran}}(\theta) = \frac{A(\theta + d\theta) - A(\theta)}{2\pi \sin(\theta)d\theta} = \frac{A'(\theta)}{2\pi \sin(\theta)}. \quad (7)$$

The radiance I of a halo due to a prescribed light path though the crystal is proportional to the surface area of the entry face of the crystal and the divergence D_{ran} divided by 4π . The proportionality factor is denoted by $T(\theta)$. $T(\theta)$ is a fraction with a value between 0 and 1. $T(\theta)$ accounts for the losses of intensity of the light rays at their passage through the crystal during the reflections/refractions at the crystal faces; it accounts for losses due to shielding of the light rays caused by the geometry of the crystals; and it accounts for the projection of the surface area of the entry face of the crystal for inclined incoming rays. These factors vary along the θ contour, and T is therefore an integral along the contour.

Then, the relation between the radiance I of a halo due to a prescribed light path though the crystal and D_{ran} is

$$I(\theta) \equiv \frac{d\sigma}{d\Omega} = a^2 T(\theta) D_{\text{ran}}(\theta), \quad (8)$$

in which a^2 is the surface area of the entry face of the crystal divided by 4π sr.

3. Four Applications

A. Simple Case: External Reflection at a Crystal Face

Figure 2 gives the deflection sphere for external reflection at a preselected crystal face. The face is put here in the equatorial ($w = 0$) plane of the sphere. Hence, colatitude ϑ of point s on the sphere corresponds to the angle of incidence i . The contours $\theta(\vartheta, \varphi)$ on the sphere follow straightforwardly from the law of reflection,

$$\theta = 180^\circ - 2i \equiv 180^\circ - 2\vartheta, \quad (9)$$

so that they consist of equidistant concentric circles with half the spacing of the colatitude circles ϑ . As the length of a contour of value ϑ is $2\pi \sin \vartheta = 2\pi \cos(\frac{1}{2}\theta)$, one has

$$dA(\theta) = 2\pi \cos(\vartheta)d\vartheta = -\pi \cos\left(\frac{1}{2}\theta\right)d\theta, \quad (10)$$

and with Eq. (7)

$$D_{\text{ran}} = \frac{\cos(\frac{1}{2}\theta)}{2 \sin(\theta)} = \frac{1}{4 \sin(\frac{1}{2}\theta)}. \quad (11)$$

Assuming for the moment reflectivity 1, then T equals the projection factor $\cos(i)$ for inclined incidence on the reflecting face. As $i = \vartheta$,

$$T(\theta) = \cos(\vartheta) = \sin\left(\frac{1}{2}\theta\right), \quad (12)$$

and thus

$$I(\theta) = a^2 T(\theta) D_{\text{ran}}(\theta) = \frac{1}{4} a^2 = \text{constant}, \quad (13)$$

indicating that the radiance I is uniformly distributed all over the celestial sphere. For reflection at (dielectric) surfaces like ice, the distribution is according to the Fresnel coefficients of reflection.

B. Double-Mirror Reflection: The Antisolar Halospot

Figure 3 shows the deflection sphere for reflection at two perpendicular mirrors. With the two mirrors in the $u = 0$ and $v = 0$ planes, the axis of the combined system coincides with the w axis of the sphere. The net effect of the reflections at the two mirrors is a 180° rotation about the w axis. Contours appear at one quadrant of the sphere, but because of the symmetry of the contours, we need to evaluate only the octant with $(u, v, w) > (0, 0, 0)$ and then to multiply the answer by two. In that octant, the colatitude ϑ of s is related to the scattering angle θ by

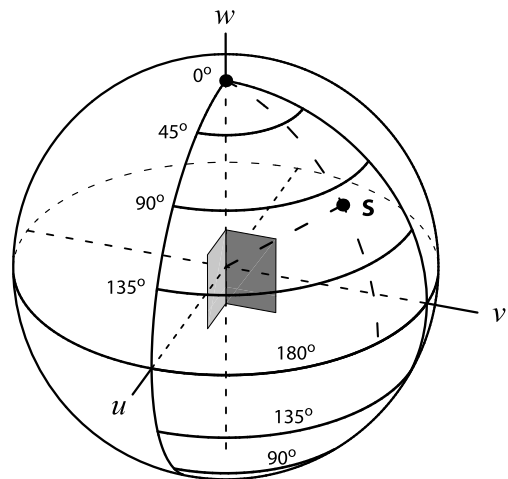


Fig. 3. Deflection sphere for reflection at two mutual perpendicular mirrors. The axis of the combined system is the w axis of the Cartesian uvw frame in which the mirrors are fixed; the mirrors are put in the $u = 0$ and $v = 0$ planes. Contours exist on only one quadrant of the sphere.

$$\theta = 2\vartheta, \quad (14)$$

so that the contours are segments of the equidistant circles like those depicted in Fig. 2 but now with a reverse counting. The length of a contour of value ϑ is $\frac{1}{2}\pi \sin \vartheta = \frac{1}{2}\pi \sin(\frac{1}{2}\theta)$ so that

$$dA(\theta) = \frac{1}{2}\pi \sin(\vartheta)d\vartheta = \frac{1}{4}\pi \sin\left(\frac{1}{2}\theta\right)d\theta, \quad (15)$$

and with Eq. (7)

$$D_{\text{ran}} = \frac{\sin(\frac{1}{2}\theta)}{8 \sin(\theta)}. \quad (16)$$

The projected area of the system scales as before (Eq. (12) with $\sin(\vartheta) = \sin(\frac{1}{2}\theta)$). Putting the reflectivity of the system at unity and $T \propto \sin(\frac{1}{2}\theta)$, we find for the radiance I

$$I(\theta) = \alpha^2 T(\theta) D_{\text{ran}}(\theta) \propto \frac{\sin^2(\frac{1}{2}\theta)}{\sin(\theta)}, \quad (17)$$

which is zero for $\theta \rightarrow 0$ but infinity for $\theta \rightarrow 180^\circ$. This singularity arises because the term $1/\sin(\theta)$ in D_{ran} Eq. (7) is not counterbalanced by the geometrical factors in T so that axial focusing occurs. As in classical glory scattering by spheres Eq. (1), the radiance distribution near $\theta = 180^\circ$ is given by

$$I(\theta \rightarrow 180^\circ) \propto \frac{1}{\sin(\theta)} \approx \frac{1}{180^\circ - \theta}. \quad (18)$$

Randomly oriented hexagonal ice crystals are capable of producing this glory analogue via light path 1321 (Tape's [18] notation), which is the path that generates in plate-oriented crystals the subparhelic circle. The resulting halo, called the antisolar halospot, manifests itself as an often somewhat

irregular spot of enhanced radiance centered at the antisolar point [19].

C. Circular Refraction Halos

1. Radiance near the Halo Angle

Figure 4 shows the contours on the deflection sphere for refraction by a prism with axis parallel with the w axis and the entry face in the $u = 0$ plane. The contours are drawn schematically; see [20] for their precise shapes. The right panel of Fig. 4 details the geometry: the colatitude of point s with respect to the u axis on the sphere corresponds to the angle of incidence i ; the $w = 0$ plane corresponds to the normal plane of the refracting prism. The inclination of the incoming ray with respect to the normal plane h and the projected angle of incidence i_p are the ordinary latitude and azimuth, respectively, of s .

The angle of incidence resulting in scattering at the halo scattering angle θ_{halo} is in the normal plane and denoted by i_{halo} . With the Bravais index of refraction, the first terms of the Taylor expansion of the prism deviation formulas for skew incidence for $\theta \rightarrow \theta_{\text{halo}}$ results in the deflection function $\theta(i, h)$ near θ_{halo} [17]:

$$\theta - \theta_{\text{halo}} \approx c_1(i_p - i_{\text{halo}})^2 + c_2 h^2, \quad (19)$$

with c_1 and c_2 constants. For the 22° ice-crystal halo, $c_1 = 0.482 \text{ rad}^{-1}$ and $c_2 = 0.169 \text{ rad}^{-1}$; for the 46° halo, $c_1 = 2.05 \text{ rad}^{-1}$ and $c_2 = 0.604 \text{ rad}^{-1}$.

Equation (19) defines $\theta(\vartheta, \varphi)$ as elliptical contours on the deflection sphere. The ellipse area is a first-order approximation at θ_{halo} of the true area $A(\theta)$ within the θ contour:

$$\lim_{\theta \rightarrow \theta_{\text{halo}}^+} \frac{1}{\theta - \theta_{\text{halo}}} \left(A(\theta) - \frac{\pi(\theta - \theta_{\text{halo}})}{\sqrt{c_1 c_2}} \right) = 0. \quad (20)$$

Then

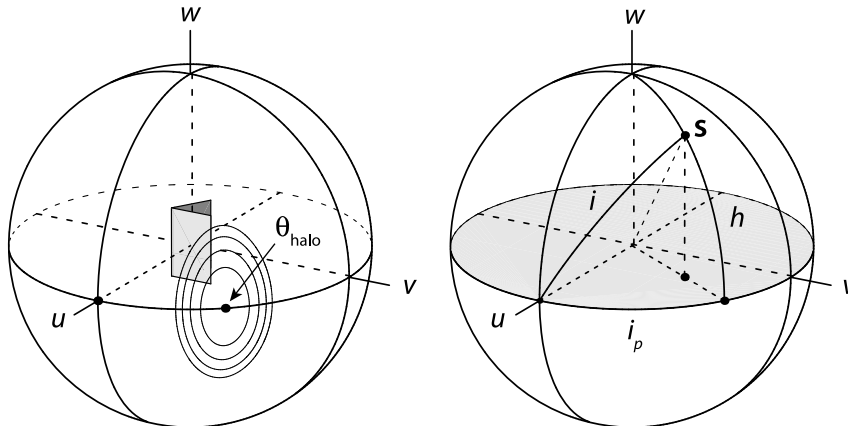


Fig. 4. Left: Deflection sphere for refraction by an (ice crystal) prism. The prism axis is parallel with the w axis of the Cartesian uvw frame in which the crystal is fixed. The entry face (light gray) is put in the $u = 0$ plane. The contours are drawn schematically; exact shapes are depicted in Figs. 9 and 13 of [20]. θ_{halo} is the halo angle. Right: Geometry of the problem, defining i , i_p , and h for a point s representing the Sun as seen in the uvw crystal frame. The $w = 0$ plane (gray) is the normal plane of the wedge.

$$A'_+(\theta_{\text{halo}}) = \lim_{\theta \rightarrow \theta_{\text{halo}}^+} \frac{A(\theta) - A(\theta_{\text{halo}})}{\theta - \theta_{\text{halo}}} = \lim_{\theta \rightarrow \theta_{\text{halo}}^+} \frac{\pi}{\sqrt{c_1 c_2}} = \frac{\pi}{\sqrt{c_1 c_2}}. \quad (21)$$

Since $D_{\text{ran}}(\theta) = A'(\theta)/(2\pi \sin(\theta))$, the right- and left-hand divergences of θ are

$$D_{\text{ran}}^+(\theta_{\text{halo}}) = \frac{1}{2\sqrt{c_1 c_2} \sin(\theta_{\text{halo}})}, \quad (22a)$$

$$D_{\text{ran}}^-(\theta_{\text{halo}}) = 0. \quad (22b)$$

Then the halo radiance $I(\theta)$ at the halo angle θ_{halo} is given by a jump:

$$I^+(\theta_{\text{halo}}) = \frac{a^2 T(\theta_{\text{halo}})}{2\sqrt{c_1 c_2} \sin(\theta_{\text{halo}})}, \quad (23a)$$

$$I^-(\theta_{\text{halo}}) = 0. \quad (23b)$$

The result [Eqs. (23)] for the radiance distribution of circular refraction halos—a jump discontinuity at θ_{halo} instead of an infinite spike—was loosely obtained in 1983 [17] and 11 years later reproduced by Berry [21].

Figure 5 shows D_{ran} , as calculated for the 22° ice crystal halo and a point Sun. Near the jump at θ_{halo} , D_{ran} decreases by 9%/degree. Of this, 4%/degree is caused by the factor $1/\sin(\theta)$ term in D_{ran} ; the remaining 5%/degree stems from the numerator of D_{ran} [Eq. (7)].

Figure 6 shows $I(\theta)$ for the circular 22° halo as calculated by a full ray-tracing program for equidimensional ice crystals and a point Sun (same run as Fig. 2 of [22]). Near θ_{halo} the simulation decreases by 25%/degree instead of by 9%/degree in Fig. 5. The

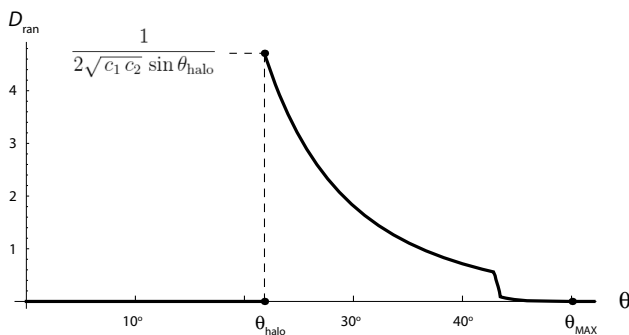


Fig. 5. Divergence D_{ran} for the 22° ice crystal halo as a function of scattering angle θ . The Sun is point shaped. The dimensionless D_{ran} is nonzero between the halo scattering angle θ_{halo} (corresponding to $\theta = 21.8^\circ$) and θ_{MAX} (50.1° , the so-called maximum deviation angle). This curve is calculated using the exact areas $A(\theta)$ [Eq. (6)] rather than any approximations. The transition to nonzero values at θ_{halo} occurs with a jump. Its values $D^+(\theta_{\text{halo}})$ and $D^-(\theta_{\text{halo}})$ agree with Eq. (22).

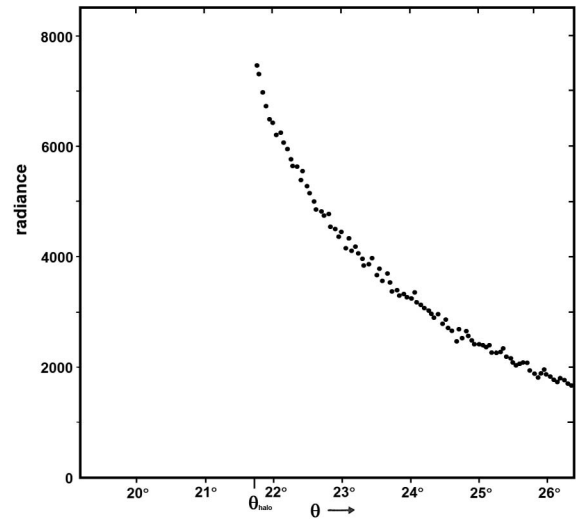


Fig. 6. Full ray-tracing simulation of the radiance as a function of scattering angle θ of a 22° circular halo generated by scattering of light from a point-shaped Sun by equidimensional crystals. The counting intervals are 0.05° wide; the unit of radiance is counts/ 0.05° .

excess decrease rate of 16%/degree compared to Fig. 5 can be attributed to shielding effects in the crystals and hence to the θ dependency of T .

2. Parhelia: Comparison of the Naive and Realistic Approaches to the Circular Halo

In what I call the “naive approach,” the circular halo is sometimes mistakenly constructed by starting from a parhelion with the Sun on the horizon and then rotating it about the Sun. The radiance distribution of the resulting circular feature, which corresponds exactly to that of the circumscribed halo for Sun in zenith, is then mistakenly conflated with the radiance distribution of the circular halo generated by randomly oriented crystals.

The radiance distribution I_{naive} of this feature is given by

$$I_{\text{naive}}(\theta) \propto \frac{I_{\text{parh}}(\theta)}{\sin(\theta)} = \frac{a^2 T(\theta) D_{\text{parh}}}{\sin(\theta)}, \quad (24)$$

where I_{parh} and D_{parh} are the radiance and the divergence for a parhelion at solar elevation zero and where the factor $1/\sin(\theta)$ accounts for the increase in solid angle with θ .

D_{parh} at θ_{halo} can be evaluated with the deflection sphere (Fig. 4). The realizable positions of the point s are now restricted to the equator of the deflection sphere (great circle at $w = 0$). Denoting the $w = 0$ great circle on the deflection sphere by S^1 , we have for the one-dimensional analogues of Eqs. (6,7)

$$l(\theta_0) = \text{length of } \{s \in S^1; \theta \leq \theta_0\}, \quad (25)$$

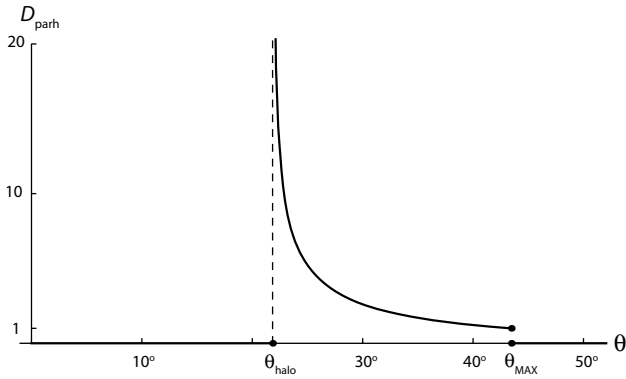


Fig. 7. Divergence D_{parh} for the 22° parheliion emerging from perfectly horizontal plate ice crystals as a function of scattering angle θ . The Sun is point shaped; solar elevation is zero. D_{parh} is nonzero between the halo scattering angle θ_{halo} (corresponding to $\theta = 21.8^\circ$) and θ_{MAX} (here 43.5°). This curve is calculated using the exact lengths $l(\theta)$ [Eq. (25)] rather than any approximations. The curve exhibits at θ_{halo} an infinite spike; at θ_{MAX} the curve jumps from 1 to 0. Note that for the entire interval $[\theta_{\text{halo}}, \theta_{\text{MAX}}]$ the values of D are higher than those for the circular halo (Fig. 5).

$$D_{\text{parh}} = \frac{l(\theta + d\theta) - l(\theta)}{d\theta} = l'(\theta). \quad (26)$$

The approximate deflection function for the parheliion is

$$\theta - \theta_{\text{halo}} \approx c_1(i - i_{\text{halo}})^2. \quad (27)$$

The parheliion analogue of Eq. (20) is

$$\lim_{\theta \rightarrow \theta_{\text{halo}}^+} \frac{1}{\theta - \theta_{\text{halo}}} \left(l(\theta) - \frac{2\sqrt{\theta - \theta_{\text{halo}}}}{\sqrt{c_1}} \right) = 0. \quad (28)$$

And, in contrast with Eq. (21),

$$\begin{aligned} l'_+(\theta_{\text{halo}}) &= \lim_{\theta \rightarrow \theta_{\text{halo}}^+} \frac{l(\theta) - l(\theta_{\text{halo}})}{\theta - \theta_{\text{halo}}} = \lim_{\theta \rightarrow \theta_{\text{halo}}^+} \frac{\pi}{\sqrt{c_1} \sqrt{\theta - \theta_{\text{halo}}}} \\ &= \infty. \end{aligned}$$

With Eq. (26), the right- and left-hand divergences of θ are

$$D_{\text{parh}}^+(\theta_{\text{halo}}) = \infty, \quad (29a)$$

$$D_{\text{parh}}^-(\theta_{\text{halo}}) = 0. \quad (29b)$$

Then the parheliion radiance $I(\theta)$ at the halo angle has an infinite spike:

$$I_{\text{parh}}^+(\theta_{\text{halo}}) = \infty, \quad (30a)$$

$$I_{\text{parh}}^-(\theta_{\text{halo}}) = 0, \quad (30b)$$

implying that the radiance of the circular halo in the naive (and misconstrued) approach $I_{\text{naive}}(\theta)$ also has an infinite spike at the halo angle rather than a jump discontinuity.

Figure 7 shows D_{parh} , as calculated for the 22° ice crystal parheliion emerging from perfectly horizontal plate crystals and a point-shaped Sun at solar elevation zero. The comparison with Fig. 5 highlights the difference between the realistic and the naive approaches to the circular halo: $I_{\text{naive}}(\theta)$ gives an infinite spike at θ_{halo} instead of a jump and predicts near θ_{halo} a stronger concentration of light.

By a comparison of a full ray-tracing simulation of the circular 22° halo with that of the circumscribed halo at Sun elevation 90° , Fig. 8 demonstrate the fundamental different nature of the radiance distribution of a circular halo according to the realistic approach and the naive approach (see, for a similar comparison, Figs. 5 and 6 of [23]).

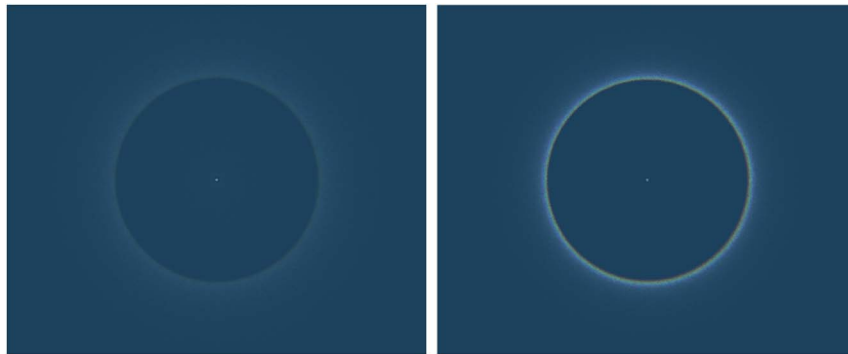


Fig. 8. Left: Ray-tracing simulation of the circular 22° halo (all crystals in random orientation). Right: Circumscribed halo for solar elevation 90° (all crystals in column orientation; dispersion in orientation C-axis = 0.1°). The crystal density is the same for both simulations. The aspect ratio c/a of the crystals is taken 2; solar disc smearing is taken into account. The radiance distribution of the circular 22° halo is smoother, and the radiance at its inner boundary is five times less than for the circumscribed halo. The right-hand panel also corresponds to a simulation of the circular 22° halo according to the naive (and misconstrued) approach.

D. Do Rainbow/Parhelia-Analogue Halos Ever Occur from Random Crystal Orientation?

A situation can be constructed in which scattering by randomly oriented crystals produces caustics similar to those that occur for parhelia and the tangent arcs to the 22° halo, that is, where the radiance has an infinite spike at θ_{halo} . This would happen, among other examples, when the deflection function of such a halo was given by

$$\theta - \theta_{\text{halo}} = [c_1(i_p - i_{\text{halo}})^2 + c_2h^2]^2 \quad (31)$$

instead of by Eq. (19). In the real world of halos, such a situation never occurs.

4. Discussion and Conclusion

There is a persistent tradition to assign to refraction halos due to random orientation the same radiance distribution as the one valid for rainbows, for parhelia, and for refraction halos due to singly oriented crystals. This custom starts in the mid-19th century when Bravais argued that the circular 22° halo should exhibit a strong (rainbow-like) accumulation of light at its inner boundary [24] and runs via authors like Garbett [25,26], Ekama [27], Pernter and Exner [28], Meyer [29], Visser [30], myself [31], Greenler [32], Lynch and Livingston [33], and Bohren and Clothiaux [5] into the present century. As shown in the present paper, the application of the halo formulas valid for preferential orientation to halos from randomly oriented crystals is not correct. The additional degree(s) of freedom in random orientation leads to a fundamental other formalism for the divergence D and hence to a different radiance distribution. A comparison of the two simulations shown in Fig. 8 highlights the nature of the difference.

From a historical standpoint it is interesting that a number of authors, apparently unaware of the difference of the radiance distributions between a parhelia and the circular 22° halo, did accidentally arrive at a radiance distribution of the circular 22° halo that is not too far from the truth by assuming that its first approximation is a step function modified with the geometric effects occurring in a regular hexagonal crystal. In this way, some researchers, e.g., Ekama [27], Visser [30], and Lynch and Schwartz [34], still used a more or less realistic radiance model in their analyses. However, the latter does not hold for Bravais [24], who applied this modified step function to parhelia.

The calculations presented in this paper, including those resulting in Figs. 6 and 7, are obtained under the assumption of ideal conditions: a point-shaped Sun and, in the case of the parhelia, perfectly horizontal plate crystals. Solar disc smearing softens the singularities and modifies the infinite parhelia spike as well as the infinite antisolar-halospot singularity into a physically more realistic finite maximum. Apart from that, the introduction of some randomness in the orientation of plate-oriented

crystals suffices to change the infinite parhelia spike into a finite maximum [17,22].

Rather than being tailored to the description of one specific halo [17,19,21], the present formalism provides a general framework for the description of any halo due to randomly oriented crystals. With the formalism, the antisolar halospot emerges in a natural way as the exact ice-crystal analogue of the ray-optics glory from backscattering by spheres. Scattering of light by randomly oriented crystals results less often in distinct halo structures than scattering by preferentially oriented crystals; the formalism provides an aid to diagnose the properties of any feature that arises from light scattering by randomly oriented crystals.

As in our previous papers dealing with a conceptual approach to halos [20,35], the formalism outlined in the present paper is not meant to compete with the computational Monte Carlo ray-tracing approach for simulating halos. Rather, the present paper is meant to complement the computational approach in order to get a better understanding of halos. In this particular case, however, it is also meant to correct a wrong concept that has been applied for ages to the calculation of radiance distribution of circular halos due to light scattering by randomly oriented crystals.

Walt Tape made important corrections to the parhelia and circular halo sections (Section 3.C) and provided the divergence plots in Figs. 5 and 7. David Maxwell (Department of Mathematical Sciences, University of Alaska, Fairbanks) proved a general result that includes Eq. (20) as a special case. The halo simulations (Fig. 8) are generated with the HaloSim program by L. Cowley and M. Schroeder [36].

References and Notes

1. The real radiance $dJ/d\Omega$ (SI units $\text{Wm}^{-2}\text{sr}^{-1}$) relates with the differential scattering cross section $d\sigma/d\Omega$ by $dJ/d\Omega = J_0 d\sigma/d\Omega NL$, where J_0 is irradiance (Wm^{-2}), N is particle density (m^{-3}), and L the length of the path of the light ray through the cloud of particles (m). Following the general custom in halo studies we call in this paper somewhat loosely $d\sigma/d\Omega$ (SI units m^2sr^{-1}) the “radiance” and denote it by symbol I .
2. H. C. van de Hulst, *Light Scattering by Small Particles* (Dover, 1981).
3. K. Liou and J. E. Hansen, “Intensity and polarization for single scattering by polydisperse spheres: a comparison of ray optics and Mie theory,” *J. Atmos. Sci.* **28**, 995–1004 (1971).
4. Semantically the term “divergence” is misleading, as large values of D lead to focusing instead of to divergence. “Convergence” or “ray density” would be better terms. Rather than introducing a new word for D we choose in this paper to stick with the unfortunate though traditional word “divergence.”
5. C. F. Bohren and E. E. Clothiaux, *Fundamentals of Atmospheric Radiation, an Introduction with 400 Problems* (Wiley, 2006).
6. K. W. Ford and J. A. Wheeler, “Semiclassical description of scattering,” *Ann. Phys.* **7**, 259–286 (1959).
7. K. W. Ford and J. A. Wheeler, “Application of semiclassical scattering analysis,” *Ann. Phys.* **7**, 287–322 (1959).
8. E. A. Mason, R. A. Munn, and F. J. Smith, “Rainbows and glories in molecular scattering,” *Endeavour* **30**, 91–96 (1971).
9. U. Buck and J. Pauly, “Determination of intermolecular potentials by the inversion of molecular beam scattering data. II.

- High resolution measurements of differential scattering cross sections and the inversion of the data for Na-Hg," *J. Chem. Phys.* **54**, 1929–1936 (1971).
10. V. N. Ostrovsky, "The giant glory effect in atomic scattering: calculations for Na-I scattering," *J. Phys. B* **8**, 2979–2986 (1975).
 11. Y. N. Demkov and J. Los, "The giant glory effect in atomic collisions," *Phys. Lett. A* **46**, 13–14 (1973).
 12. Y. N. Demkov and V. N. Ostrovsky, "Enhanced backscattering in antiproton-atom collision: coulomb glory," *J. Phys. B* **34**, L595–L599 (2001).
 13. A noticeable exception is primary rainbow scattering for refraction index $n = \sqrt{2}$ where the angle of reflection of the Descartes ray occurs at the Brewster angle. Then, for polarization perpendicular to the scattering plane $T(\theta) \propto \theta - \theta_r$, resulting near the rainbow angle in a square-root radiance distribution $I(\theta) \propto (\theta - \theta_r)^{+1/2}$ instead of in the inverse square-root distribution given by Eq. (3).
 14. W. Tape, "Analytic foundations of halo theory," *J. Opt. Soc. Am.* **70**, 1175–1192 (1980).
 15. M. V. Berry and S. Klein, "Diffraction near fake caustics," *Eur. J. Phys.* **18**, 303–306 (1997).
 16. R. A. R. Tricker, *Introduction to Meteorological Optics* (American Elsevier, 1970).
 17. G. P. Können, "Polarisation and intensity distributions of refraction halos," *J. Opt. Soc. Am.* **73**, 1629–1640 (1983).
 18. W. Tape, *Atmospheric Halos*, Vol. 64 of Antarctic Research Series (American Geophysical Union, 1994).
 19. G. P. Können, M. Bodó, and Á. Kiricsi, "Antisolar halospot," *Appl. Opt.* **47**, H167–H170 (2008).
 20. W. Tape and G. P. Können, "A general setting for halo theory," *Appl. Opt.* **38**, 1552–1625 (1999).
 21. M. V. Berry, "Supernumerary ice crystal halos?" *Appl. Opt.* **33**, 4563–4568 (1994).
 22. G. P. Können and J. Tinbergen, "Polarimetry of a 22° halo," *Appl. Opt.* **30**, 3382–3400 (1991).
 23. G. P. Können, "The prodigious halo of the other Huygens," *Appl. Opt.* **54**, B185–B193 (2015).
 24. A. Bravais, "Mémoire sur les halos et les phénomènes optiques qui les accompagnent," *J. de l'École Royale Polytechnique* **31**, 1–270 (1847).
 25. E. L. Garbett, "Description of some Parhelia seen at Portsea on the 29th of March 1848; with some remarks on these phenomena generally," *Philos. Mag.* **32**(217), 434–446 (1848).
 26. Garbett's halo simulation device [25] consisting of rotating black wheel with seven colored figures pasted on it (his Fig. 4), each of them shaped according to the radiance distribution of a parhelion, does not simulate the 22° halo (as claimed) but the circumscribed halo for solar elevation 90° instead (as our Fig. 8, right). So it shows the circular 22° halo according to the naive approach instead of the real circular 22° halo. If Garbett had made for each color a set of several identical figures instead of one and had pasted each set of identically colored figures in the shape of a tangent arc for solar elevation 0° on his wheel, then upon rotation he would have obtained a correct simulation of the circular 22° halo.
 27. H. Ekama, "Mijne waarnemingen omtrent de halo, verricht in de Kara zee gedurende de overwintering 1882-1883," Ph.D. dissertation (University of Leiden, 1884).
 28. J. M. Pernter and F. M. Exner, *Meteorologische Optik*, 2nd ed. (Wilhelm Braumüller, 1922).
 29. R. Meyer, *Die Haloerscheinungen* (Henri Grand, 1929).
 30. S. W. Visser, "On the diffraction of light in the formation of halos," *Proc. Roy. Ac. Sc.* **19**, 1174–1196 (1917).
 31. G. P. Können, "Overeenkomsten en verschillen tussen deeltjesstrooiing en lichtstrooiing," *Ned. Tijdschr. Natuurkd.* **38**, 265–271 (1972).
 32. R. Greenler, *Rainbows, Halos, and Glories* (Cambridge University, 1980), p. 25.
 33. D. K. Lynch and W. Livingston, *Color and Light in Nature* (Cambridge University, 1995), p. 159.
 34. D. K. Lynch and P. Schwartz, "Intensity profile of the 22° halo," *J. Opt. Soc. Am. A* **2**, 584–589 (1985).
 35. G. P. Können, "Symmetry in halo displays and symmetry in halo-making crystals," *Appl. Opt.* **42**, 318–331 (2003).
 36. L. Cowley and M. Schroeder, "HaloSim simulation program," <http://www.atoptics.co.uk/halo/halfeat.htm>.